

Coherent Curvature Radiation Spectrum by Dynamically Fluctuating Bunches in Magnetospheres

Yuan-Pei Yang^{1,2*} and Bing Zhang^{3,4†}

¹South-Western Institute for Astronomy Research, Yunnan University, Kunming, Yunnan 650504, China

²Purple Mountain Observatory, Chinese Academy of Sciences, Nanjing 210023, China

³Nevada Center for Astrophysics, University of Nevada, Las Vegas, NV 89154, USA

⁴Department of Physics and Astronomy, University of Nevada, Las Vegas, NV 89154, USA

Accepted XXX. Received YYY; in original form ZZZ

ABSTRACT

Coherent curvature radiation by charged bunches has been discussed as the radiation mechanism for radio pulsars and fast radio bursts. Important issues for this radiation mechanism include how the bunches form and disperse in the magnetosphere of a pulsar or magnetar. More likely, bunches form and disperse continuously and it remains unclear what the spectral features are for these fluctuating bunches. In this work, we consider that the bunches in a magnetosphere have a formation rate of λ_B , a lifetime of τ_B , and a typical Lorentz factor of γ , and analyze the spectral features of coherent curvature radiation by these fluctuating bunches. We find that the emission spectrum by a single fluctuating bunch is suppressed by a factor of $\sim (\lambda_B \tau_B)^2$ compared with that of a single persistent bunch, and there is a quasi-white noise in a wider band in the frequency domain. The high-frequency cutoff of the spectrum is at $\sim \max(\omega_c, 2\gamma^2/\tau_B)$, where ω_c is the typical frequency of curvature radiation. If the observed spectrum is not white-noise-like, the condition of $2\gamma^2 \lambda_B \gtrsim \min(\omega_c, 2\gamma^2/\tau_B)$ would be required. On the other hand, due to the random fluctuation of bunches, the radiation by multiple fluctuating bunches along a field line is the incoherent summation of the radiation by single bunches, and the spectral shape is the same as that of a single bunch. We further discuss the effects of bunch structures and some possible mechanisms of bunch formation and dispersion.

Key words:

radiation mechanisms: non-thermal – radio continuum: general – (transients:) fast radio bursts – (stars:) pulsars: general

1 INTRODUCTION

The brightness temperatures of both radio pulsars and fast radio bursts (FRBs) are extremely high and are much greater than any plausible thermal temperature of the emitting electrons (e.g., Melrose 2017; Petroff et al. 2019; Cordes & Chatterjee 2019; Zhang 2020, 2022a; Xiao et al. 2021; Lyubarsky 2021; Bailes 2022). This suggests that the radiation mechanism of radio pulsars and FRBs must be coherent. For incoherent waves with random phases, the amplitude square of their superposition is approximately the sum of the amplitude squares of each wave. Thus, the observed emission power would be the simple summation of the emission power of individual charged particles, as proposed in most astrophysical scenarios. For coherent waves with certain phase differences, the amplitude square of their superposition could be significantly enhanced or reduced due to the wave coherent superposition process. In particular, “coherently enhanced” waves usually require that the phase differences of superposing waves must be much less the half wavelength of the waves. In the literature about radiation mechanism, “coherent” is mainly defined as “coherently enhanced”.

Some coherent emission mechanisms have been invoked to interpret the emissions of radio pulsars and FRBs (e.g., Melrose 2017; Zhang 2022a): coherent radiation by charged bunches (i.e., antenna mechanism), maser by hydrodynamic instabilities or kinetic instabilities, etc. In this paper, we mainly focus on coherent curvature radiation by charged bunches that has been proposed as one of the popular ideas to explain the emission of pulsars (Sturrock 1971; Ginzburg & Zhelezniakov 1975; Ruderman & Sutherland 1975; Buschauer & Benford 1976; Benford & Buschauer 1977; Melikidze et al. 2000; Gil et al. 2004; Basu et al. 2022) and FRBs (Katz 2014, 2018; Kumar et al. 2017; Lu & Kumar 2018; Yang & Zhang 2018b; Kumar & Bošnjak 2020; Lu et al. 2020; Yang et al. 2020; Cooper & Wijers 2021; Wang et al. 2022a,b; Tong & Wang 2022; Liu et al. 2022; Qu et al. 2023). Due to the two-stream instabilities in the magnetosphere of a neutron star, charged bunches might form and radiate electromagnetic radiation coherently (Ruderman 1971; Benford & Buschauer 1977; Cheng & Ruderman 1980; Usov 1987; Kumar et al. 2022). However, as pointed out by some authors (e.g., Melrose 2017; Lyubarsky 2021), these models involving charged bunches have some important issues: (1) The charged bunches might be short-lived; (2) The radiation might be strongly suppressed by the magnetosphere plasma. For the latter issue, Gil et al. (2004) and Lyubarsky (2021) pointed out that electromagnetic waves with frequencies below the plasma frequency could propagate in the highly magnetized plasma in the

* E-mail: ypyang@ynu.edu.cn (YPY)

† E-mail: bing.zhang@unlv.edu (BZ)

magnetosphere, but the radiation power would be significantly suppressed. However, [Qu et al. \(2023\)](#) recently found that the plasma suppression effect could be ignored in the case of FRBs because of the existence of a parallel electric field in the FRB emission region, as is required to power the bright FRB emission. The former issue leads to a more fundamental question: Is it necessary that the charged bunches have to be long-lived in order to explain the observed features of radio pulsars and FRBs? In other words, how do the formation and dispersion of bunches affect the observed radiation?

In this work, we will analyze the spectral features of the coherent curvature radiation by dynamically fluctuating bunches in the magnetosphere of a neutron star. We consider that the bunches in the magnetosphere form with an average rate of λ_B and have an average lifetime of τ_B , and discuss how λ_B and τ_B affect the radiation spectral feature. The paper is organized as follows. In Section 2, we discuss the brightness temperature of the curvature radiation in a magnetosphere using a more physical treatment. In Section 3, we analyze the spectral features of coherent curvature radiation by fluctuating bunches, including the features by a single persistent bunch with different structures (Section 3.1), a single fluctuating bunch (Section 3.2), and multiple fluctuating bunches (Section 3.3). In Section 4, we discuss the formation and dispersion mechanisms of bunches in the magnetosphere and calculate λ_B and τ_B in various physical scenarios. The results are summarized and discussed in Section 5. The convention $Q_x = Q/10^x$ is adopted in cgs units unless otherwise specified.

2 BRIGHTNESS TEMPERATURE OF COHERENT CURVATURE RADIATION IN A MAGNETOSPHERE: A PHYSICAL TREATMENT

Before discussing the spectral features of coherent curvature radiation by charged bunches, we first point out that the physical brightness temperature in such a scenario is different from the standard definition. The flux-intensity relation is generally given by $F_\nu = \pi I_\nu (l_e/d)^2$, where l_e is emphasized to be *the emission region scale perpendicular to the line of sight*, d is the distance between source and observer. Since the brightness temperature, T_B , is defined by the Rayleigh-Jeans law as $I_\nu = 2\nu^2 k_B T_B / c^2$, it can be written as

$$T_B \simeq \frac{c^2}{2\pi k_B \nu^2} \left(\frac{d}{l_e} \right)^2 F_\nu, \quad (1)$$

where ν is the frequency of the electromagnetic wave. If the emission region satisfies the following conditions: (1) The emission region is non-relativistic; (2) Its perpendicular scale is the same order of magnitude as the transverse scale; (3) The radiation is isotropic at any point of the emission region; l_e could be estimated by the observed duration Δt of a transient, i.e., $l_e \sim c\Delta t$, and the classical formula for the brightness temperature is obtained,

$$T_B \simeq \frac{1}{2\pi k_B} \left(\frac{d}{\nu \Delta t} \right)^2 F_\nu = 10^{35} \text{ K } d_{\text{Gpc}}^2 \nu_9^{-2} \Delta t_{-3}^{-2} F_{\nu, \text{Jy}}, \quad (2)$$

where $d_{\text{Gpc}} = d/1 \text{ Gpc}^1$ and $F_{\nu, \text{Jy}} = F_\nu/1 \text{ Jy}$. Once the distance d is obtained, the brightness temperature could be directly estimated (e.g., [Xiao & Dai 2022](#); [Luo et al. 2023](#); [Zhu-Ge et al. 2023](#)).

¹ Here we do not specify whether d is luminosity distance or angular diameter distance for an order of magnitude estimate. A more precise treatment involves a correction factor with a certain power of $(1+z)$, see [Luo et al. \(2023\)](#) and [Zhang \(2022a\)](#) for details.

However, if the emission region is within a magnetosphere and charged particles are relativistic, as are envisaged in many theoretical models of radio pulsars and FRBs (e.g., [Sturrock 1971](#); [Ruderman & Sutherland 1975](#); [Kumar et al. 2017](#); [Yang & Zhang 2018b](#); [Lu et al. 2020](#)), the above condition (2) and (3) would not be satisfied. We consider that the charged particles/bunches are relativistically moving with a Lorentz factor γ along the curved field lines with a curvature radius ρ . For $\omega \lesssim \omega_c$, where $\omega_c \sim \gamma^3 c/\rho$ is the typical frequency of curvature radiation, the radiation beaming angle at the angular frequency ω is approximately ([Jackson 1998](#))

$$\theta_e(\omega) \sim \frac{1}{\gamma} \left(\frac{\omega_c}{\omega} \right)^{1/3}, \quad (3)$$

which involves the field line direction. Thus, the transverse length-scale l_e of the emission region at the distance r from the neutron star center should be estimated by

$$\begin{aligned} l_e &\sim r\theta_e(\omega) \sim \frac{3}{4} \rho \theta_e(\omega) \\ &\sim \frac{3}{4} \theta \left(\frac{c\rho^2}{\omega} \right)^{1/3} \simeq 2.7 \times 10^5 \text{ cm } \rho_8^{2/3} \nu_9^{-1/3} \theta, \end{aligned} \quad (4)$$

where $\rho \simeq 4r/3\theta$ is the curvature radius at the position (r, θ) , and θ is the poloidal angle between the emission region and the magnetic axis. We can see that for the above typical parameters, the transverse lengthscale l_e is much smaller than that estimated by $c\Delta t \sim 3 \times 10^7 \text{ cm } \Delta t_{-3}$. As a result, a more physical brightness temperature for the curvature radiation can be estimated as

$$\begin{aligned} T_B &= \frac{32\pi}{9k_B} \left(\frac{d}{\theta} \right)^2 \left(\frac{c}{\rho\omega} \right)^{4/3} F_\nu \\ &= 1.3 \times 10^{39} \text{ K } d_{\text{Gpc}}^2 \theta^{-2} \rho_8^{-4/3} \nu_9^{-4/3} F_{\nu, \text{Jy}}. \end{aligned} \quad (5)$$

One can see that for curvature radiation in a magnetosphere, the brightness temperature should depend on the emission region parameters (ρ, θ) . For typical parameters, the brightness temperature is much higher than the value estimated by the classical formula Eq.(2). Meanwhile, it is worth noting that such a brightness temperature is independent of the burst duration Δt . The reason is that the burst duration does not directly reflect the transverse size of the emission region.

3 COHERENT CURVATURE RADIATION BY FLUCTUATING BUNCHES

Charged bunches are thought to be formed by certain plasma instabilities in the magnetosphere, e.g., two-stream instability ([Ruderman & Sutherland 1975](#); [Benford & Buschauer 1977](#); [Cheng & Ruderman 1980](#); [Usov 1987](#)), and the bunch formation rate λ_B could be estimated by the growth rate of the plasma instability. Since the bunch is charged, over-dense, and composed of particles with different velocities, it would be dispersed by plasma instabilities, electrostatic repulsion, velocity dispersion, radiation cooling, etc. In this section, we mainly calculate the spectrum of the coherent curvature radiation by fluctuating bunches and discuss how the spectral feature is affected by the bunch formation and dispersion.

3.1 Radiation by a single persistent bunch with different structures

First, we briefly summarize the spectral properties of a single persistent bunch. We consider that the bunch has the velocity ν with

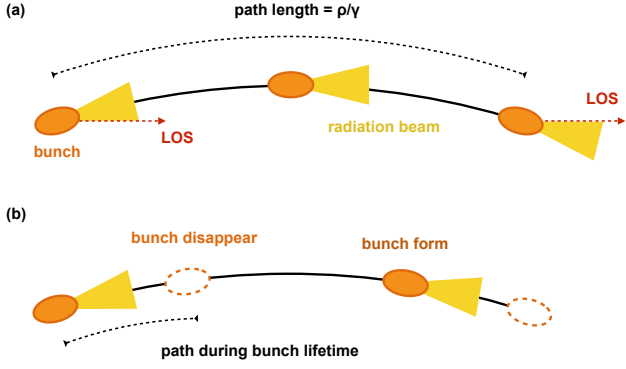


Figure 1. Schematic configurations of a bunch moving along a magnetic field line and emitting curvature radiation. The black line denotes the magnetic field line, the orange ellipse denotes the bunch, the dashed ellipse denotes the bunch disappearing due to dispersion, and the yellow region denotes the radiation by the bunch due to relativistic motion. Panel (a): the bunch is persistent. Due to the relativistic motion of the bunch, the length scale of the path along the line of sight (LOS) is ρ/γ , where ρ is the curvature radius of the field line, and γ is the bunch Lorentz factor. (b) the bunch is fluctuating due to rapid formation and dispersion when the building plasma moves along the field line.

Lorentz factor $\gamma = (1 - v^2/c^2)^{-1/2}$ and moves along the magnetic field line with a curvature radius ρ , as shown in the panel (a) of Figure 1.

If the bunch lifetime is long enough, $\tau_B > \rho/\gamma c$, which is comparable to the time of a persistent bunch sliding along a curved magnetic field line, the observer will see the radiation with the emission cone of angular width $\sim 1/\gamma$ around the observer direction, and the typical angular frequency of the emission wave is

$$\omega_c = \frac{1}{\tau_c} \sim \left[\frac{\rho}{\gamma c} \left(1 - \frac{v}{c} \right) \right]^{-1} \approx \frac{2\gamma^3 c}{\rho}, \quad (6)$$

where τ_c is the typical pulse duration of the classical curvature radiation for a single point source, and the factor of $(1 - v/c)$ is due to the propagation time-delay effect.

We consider that the classical curvature radiation is in the form of a finite pulse $E(t)$, and $E(t)$ vanishes sufficiently rapidly for $t \rightarrow \pm\infty$. For convenience, we define $A(t) \equiv (c/4\pi)^{1/2} [RE(t)]_{\text{ret}}$, where R is the distance between the observer and the bunch at the retarded time, and the bracket $[\dots]_{\text{ret}}$ is evaluated at the retarded time. The Fourier transform of $A(t)$ is defined as

$$A(\omega) = \frac{1}{\sqrt{2\pi}} \int_{-\infty}^{\infty} A(t) e^{i\omega t} dt, \quad (7)$$

$$A(t) = \frac{1}{\sqrt{2\pi}} \int_{-\infty}^{\infty} A(\omega) e^{-i\omega t} d\omega. \quad (8)$$

Here we adopt the above definitions of Fourier transforms as the same as those in Jackson (1998), and the corresponding properties of Fourier transform will be adopted accordingly in the following discussion. The directional emission spectrum (defined as *the radiation energy per unit solid angle per unit angular frequency*) is (Jackson 1998)

$$P_A(\omega) \equiv \frac{dW}{d\Omega d\omega} = 2|A(\omega)|^2 = \frac{c}{4\pi^2} \left| \int_{-\infty}^{\infty} [RE(t)]_{\text{ret}} e^{i\omega t} dt \right|^2. \quad (9)$$

For the curvature radiation by a single persistent bunch, the properties of $P_A(\omega)$ mainly depend on the spatial structure of the charged bunch (Yang & Zhang 2018b; Yang et al. 2020). Here, we briefly

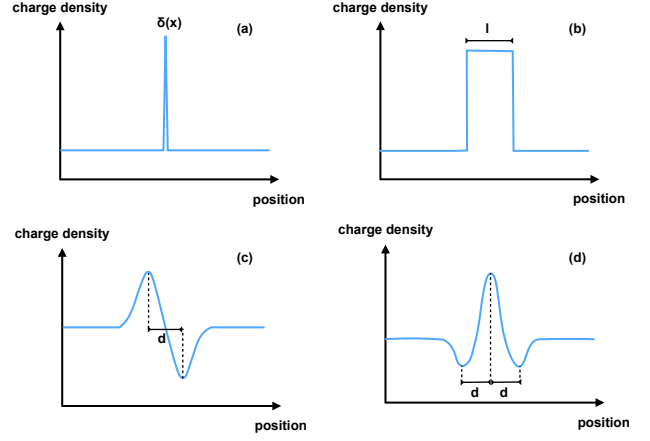


Figure 2. Charge density distributions for different bunch structures. Panel (a): A single point-source bunch, with the charge density described by a delta function $\delta(x)$; Panel (b): A one-dimensional bunch with lengthscale l , with a uniform charge density; Panel (c): A bunch-cavity pair formed in a plasma background, with the separation between the bunch and the cavity being d . Panel (d): A bunch-cavity system satisfying the structures of a soliton, with the separations between the bunch and the cavities being d .

summarize the following three scenarios with the different structures as shown in Figure 2:

1. A point-source bunch (see the panel (a) of Figure 2): If the bunch length is much smaller than a half wavelength, the point-source approximation is reasonable. The emission spectrum of the curvature radiation is (Jackson 1998; Yang & Zhang 2018b)

$$P_A(\omega) \propto \omega^{2/3} e^{-\omega/\omega_c}. \quad (10)$$

In particular, the spectral index of $2/3$ is due to the angular spectrum involved in curvature radiation, which is different from the scenario of synchrotron radiation that is usually described by total spectrum with a spectral index of $1/3$, except the case with a narrow pitch-angle distribution (Yang & Zhang 2018a). The emission spectrum is shown by the black curve in Figure 3.

2. A one-dimensional bunch with a finite length l (see the panel (b) of Figure 2): The corresponding emission spectrum of curvature radiation is (Yang & Zhang 2018b)

$$P_A(\omega) \propto \text{sinc}^2\left(\frac{\omega}{\omega_l}\right) \omega^{2/3} e^{-\omega/\omega_c} \quad \text{with } \omega_l \approx 2c/l, \quad (11)$$

where $\text{sinc}(x) \equiv \sin x/x$. Here the charge distribution of the bunch is assumed to be uniform. If $\omega \gg \omega_l$, one has $\text{sinc}^2(\omega/\omega_l) \sim \omega^{-2}$ due to the rapid oscillation of the term $\text{sinc}^2(\omega/\omega_l)$ with a unit amplitude in the sinc function, leading to a softer spectrum compared with that of a point source. The emission spectrum is shown by the red curve in Figure 3. In particular, when $\omega_l < \omega_c$, the peak radiation specific power would be suppressed by a factor of $\sim (\omega_l/\omega_c)^{2/3}$, leading to the total radiation energy suppressed by a factor

$$\eta_l \approx \frac{\omega_l P_A(\omega_l)}{\omega_c P_A(\omega_c)} \approx \left(\frac{\omega_l}{\omega_c} \right)^{5/3} \approx 0.9 I_1^{-5/3} v_{c,9}^{-5/3}, \quad (12)$$

compared with that of a point source given by Eq.(10). This formula can be used to estimate how the bunch length suppresses the total radiation power.

3. A bunch-cavity pair or similar system formed by plasma background fluctuation (see panel (c) and panel (d) of Figure 2). First, we consider that a charged bunch forms in the plasma background and

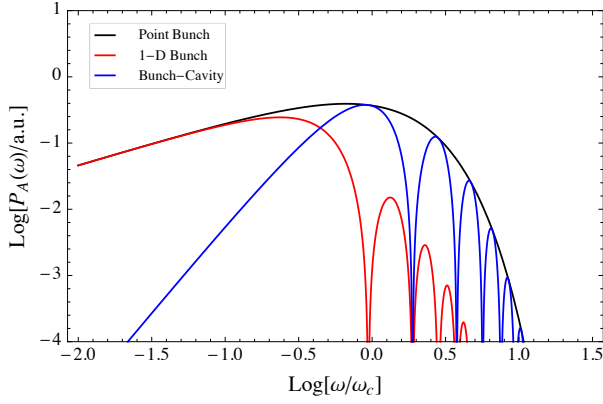


Figure 3. The emission spectrum of a single persistent bunch. The black, red, and blue curves correspond to the emission spectrum of a point-source bunch (panel (a) in Figure 2), a one-dimensional bunch with $\omega_l = 0.3\omega_c$ (panel (b) in Figure 2), a bunch-cavity system (a bunch-cavity pair (panel (c) in Figure 2) or a soliton (panel (d) in Figure 2)) with $\omega_d = 0.3\omega_c$, respectively. The unit of the emission spectrum is arbitrary. For easy comparison with the spectral shapes of different scenarios, the emission spectrum of the bunch-cavity system is suppressed by an arbitrary factor in this figure.

has a charge density larger than the background, then a corresponding cavity with a charge density smaller than the background would form near the bunch, as shown in panel (c) of Figure 2. For simplicity, we treat the bunch-cavity pair as a two-point source with a separation d . Thus, the charge density distribution of the bunch-cavity pair system could be described by $\rho_{bc}(x) = q\delta(x) - q\delta(x-d) + \rho_0$, where x denotes the pair position, $\pm q$ in the first two terms correspond to the charges of the bunch and the cavity, respectively, and ρ_0 is the charge density of the plasma background. Since a persistent current (i.e., plasma background) cannot generate electromagnetic waves (Yang & Zhang 2018b), only the first two terms contribute to the radiation. Therefore, the radiation of the bunch-cavity pair is consistent with that of a separated electron/positron pair discussed by Yang et al. (2020). Based on the charge density distribution, the pulse profile is given by $A(t) = A_0(t) - A_0(t-d/c)$, where $A_0(t)$ and $-A_0(t-d/c)$ correspond to the pulse profiles of the bunch and the cavity, respectively. According to the time-shifting property of the Fourier transform, one has $A(\omega) = A_0(\omega) - A_0(\omega)e^{i\omega d/c}$. Using $P_A(\omega) = 2|A(\omega)|^2$ by Eq.(9), one has (Yang et al. 2020)

$$P_A(\omega) \propto 2 \left[1 - \cos\left(\frac{\omega}{\omega_d}\right) \right] \omega^{2/3} e^{-\omega/\omega_c} \quad \text{with } \omega_d \simeq c/d. \quad (13)$$

For $\omega \ll \omega_d$, one has $1 - \cos(\omega/\omega_d) \propto \omega^2$, leading to $P_A(\omega) \propto \omega^{8/3}$ at the low-frequency band. Thus, the radiation spectrum is much narrower and harder than that of a point source given by Eq.(10). The emission spectrum is shown by the blue curve in Figure 3. Furthermore, it can be further proved that the above formula is also available for some more complex bunch-cavity systems. For example, Melikidze et al. (2000) proposed that some plasma solitons with net charges will result from a ponderomotive Miller force. Each soliton consists of one large bunch and two small cavities (see Figure 2 in Melikidze et al. (2000) and panel (d) of Figure 2), because the excess of one charge is compensated by the lack of this charge in the nearby regions. The charge density distribution of the bunch-cavity system could be roughly described by $\rho_{bc}(x) = -q\delta(x-d) + 2q\delta(x) - q\delta(x+d) + \rho_0$. Similar to the calculation of the bunch-cavity pair, the same result as Eq.(13) is obtained, as shown by the blue curve in Figure 3.

The above discussion assumes that the particles in the bunch have

a Lorentz factor γ . If the energy distribution of the charged particles satisfies a power-law distribution, the corresponding radiation spectrum would be characterized by a multi-segment broken power-law, and the details have been discussed in Yang & Zhang (2018b).

3.2 Radiation by a single fluctuating bunch

If the bunch lifetime is short, $\tau_B < \rho/\gamma c$, the observed pulse duration will be shorter than τ_c given by Eq.(6), leading to a higher typical frequency than that of classical curvature radiation, i.e.

$$\tilde{\omega}_c \sim \left[\tau_B \left(1 - \frac{v}{c} \right) \right]^{-1} \sim \frac{2\gamma^2}{\tau_B}. \quad (14)$$

Therefore, a fluctuating bunch with a short lifetime will generate electromagnetic radiation with a higher frequency than the typical frequency of classical curvature radiation.

We consider that a bunch forms and disperses intermittently when the building particles move along a field line, and the coherent radiation pulses are generated when the bunch exists, as shown in panel (b) of Figure 1. The bunch forms with a rate of λ_B and disperses during a lifetime of τ_B . Due to the relativistic motion of the building particles with $\gamma \gg 1$, the pulse rate λ_b and the pulse duration τ_b should be corrected by the propagation time-delay effect, i.e.

$$\lambda_b = \left(1 - \frac{v}{c} \right)^{-1} \lambda_B \simeq 2\gamma^2 \lambda_B, \quad (15)$$

$$\tau_b = \left(1 - \frac{v}{c} \right) \tau_B \simeq \frac{\tau_B}{2\gamma^2} \sim \tilde{\omega}_c^{-1}, \quad (16)$$

where the factor of $(1 - v/c)$ is due to the propagation time-delay effect.

During the time of $\rho/\gamma c$ when the emission cone sweeps the observing direction, the bunch would disperse and generate multiple times when the building plasma particles move along the magnetic field line. We consider that the radiation is in the form of $\tilde{A}(t)$. When the bunch exists, $\tilde{A}(t) \simeq A(t)$, where $A(t)$ is the radiation form of the classical curvature radiation by a single persistent source, as discussed in Section 3.1; when the bunch disappears, $\tilde{A}(t) \simeq 0$. Therefore, the form of $\tilde{A}(t)$ can be written as

$$\tilde{A}(t) = A(t)S(t), \quad (17)$$

where $S(t)$ is the pulse sampling function with

$$S(t) = \begin{cases} 1, & \text{for bunch existing,} \\ 0, & \text{for bunch disappearing,} \end{cases} \\ = \sum_k s(t - t_k) \quad (18)$$

and

$$s(t) = \begin{cases} 1, & \text{for } 0 \leq t \leq \tau_b, \\ 0, & \text{otherwise.} \end{cases} \quad (19)$$

Here t_k corresponds to the starting time of the k -th bunch generation, and τ_b is the pulse duration from a bunch. The pulse sampling function $S(t)$ is shown in Figure 4.

We assume that pulse generation satisfies a Poisson process, thus, the probability to generate k pulses during time t is

$$P_k(t) = \frac{(\lambda_b t)^k}{k!} e^{-\lambda_b t}, \quad (20)$$

where $\lambda_b = 2\gamma^2 \lambda_B$ is the pulse rate that is corrected for the propagation time-delay effect. Here $\{t_k\}$ in Eq.(18) is distributed in a Poisson

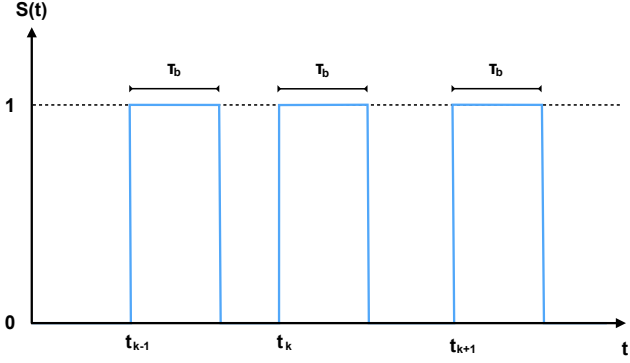


Figure 4. The pulse sampling function $S(t)$ given by Eq.(18). $\{t_k\}$ is the starting time of the k -th pulse. Each pulse has a duration of τ_b .

distribution with the parameter λ_b , and the probability density function of $\{t_k\}$ is related to the probability that the k -th point occurs in a short interval at the arbitrary time t for short Δt ,

$$\begin{aligned} P_{t_k}(t)\Delta t &= P(t < t_k < t + \Delta t) \\ &= P_{k-1}(t)P_1(\Delta t) = P_{k-1}(t)\lambda_b\Delta t. \end{aligned} \quad (21)$$

Thus, one obtains the probability density function for $\{t_k\}$, i.e.

$$P_{t_k}(t) = \lambda_b P_{k-1}(t). \quad (22)$$

Before calculating the emission spectrum $P_{\tilde{A}}(\omega)$ of $\tilde{A}(t)$, we are first interested in its autocorrelation function $R_{\tilde{A}}(\tau)$. Since $S(t)$ corresponds to a random sampling process, $R_{\tilde{A}}(\tau)$ could be described by

$$\begin{aligned} R_{\tilde{A}}(\tau) &= \mathcal{E}[\tilde{A}(t) * \tilde{A}^\dagger(-t)] = \mathcal{E}[(A(t)S(t)) * (A(-t)S(-t))^\dagger] \\ &= \mathcal{E}\left[\int A(t+\tau)S(t+\tau)A^\dagger(t)S^\dagger(t)dt\right] \\ &= \int A(t+\tau)A^\dagger(t)\mathcal{E}[S(t+\tau)S^\dagger(t)]dt, \end{aligned} \quad (23)$$

where $\tilde{A}(t) * \tilde{A}^\dagger(-t)$ denotes the autocorrelation function of $\tilde{A}(t)$, and $\mathcal{E}[X]$ denotes the expectation of the random variable X involved by the random process. The integral range is from $-\infty$ to ∞ , the symbol “*” denotes the convolution operator, and the superscript “ \dagger ” denotes the conjugation. In the above calculation, the property of $\int f(t)f^\dagger(t-\tau)dt = \int f(t+\tau)f^\dagger(t)dt$ is used based on variable substitution $t-\tau \rightarrow t$. For the Poisson sampling process, the autocorrelation of $R_S(\tau)$ satisfies (Franks 1981)

$$\begin{aligned} R_S(\tau) &= \mathcal{E}[S(t+\tau)S^\dagger(t)] = \sum_k \sum_j \mathcal{E}[s(t+\tau-t_k)s(t-t_j)] \\ &= \sum_{k=j} \int s(t+\tau-\xi)s(t-\xi)p_{t_k}(\xi)d\xi \\ &+ \sum_{k \neq j} \int s(t+\tau-\eta)p_{t_k}(\eta)d\eta \int s(t-\sigma)p_{t_k}(\sigma)d\sigma \\ &= (\lambda_b q_s)^2 + \lambda_b r_s(\tau), \end{aligned} \quad (24)$$

where

$$q_s \equiv \int s(t)dt, \quad (25)$$

$$r_s(\tau) \equiv \int s(t+\tau)s(t)dt. \quad (26)$$

Notice that both $S(t)$ and $s(t)$ are real functions according to Eq.(18)

and Eq.(19). Since the autocorrelation function $R_S(\tau)$ is independent of t (i.e., a wide-sense-stationary process), Eq.(23) could be finally written as

$$R_{\tilde{A}}(\tau) = R_A(\tau)R_S(\tau), \quad (27)$$

where $R_A(\tau)$ is the autocorrelation function of $A(t)$. Therefore, the autocorrelation function of the product of $A(t)$ and $S(t)$ is the product of the autocorrelation of each one.

The emission spectrum of $\tilde{A}(t)$ is given by Eq.(9),

$$P_{\tilde{A}}(\omega) \equiv \frac{d\tilde{W}}{d\Omega d\omega} = 2|\tilde{A}(\omega)|^2. \quad (28)$$

According to the convolution theorem and conjugation property of Fourier transform, $|\tilde{A}(\omega)|^2$ could be written as

$$\begin{aligned} |\tilde{A}(\omega)|^2 &= \tilde{A}(\omega)\tilde{A}^\dagger(\omega) \\ &= \frac{1}{\sqrt{2\pi}}\mathcal{F}(\tilde{A}(t) * \tilde{A}^\dagger(-t)) = \frac{1}{\sqrt{2\pi}}\mathcal{F}(R_{\tilde{A}}(\tau)), \end{aligned} \quad (29)$$

where $\mathcal{F}(\dots)$ denotes the Fourier transform, the factor of $1/\sqrt{2\pi}$ is involved due to the definition of Fourier transform Eq.(7) and Eq.(8). Thus, the Fourier transform of the autocorrelation function is the power spectrum, known as Wiener-Khinchin’s theorem. According to Eq.(27), Eq.(28), Eq.(29) and the convolution theorem, the emission spectrum of $\tilde{A}(t)$ could be finally written as

$$\begin{aligned} P_{\tilde{A}}(\omega) &= \frac{2}{\sqrt{2\pi}}\mathcal{F}(R_A(\tau)R_S(\tau)) = 2|A(\omega)|^2 * \frac{1}{\sqrt{2\pi}}\mathcal{F}(R_S(\tau)) \\ &= P_A(\omega) * P_S(\omega), \end{aligned} \quad (30)$$

where $\mathcal{F}(R_A(\tau)R_S(\tau)) = (1/\sqrt{2\pi})\mathcal{F}(R_A(\tau)) * \mathcal{F}(R_S(\tau))$ is used, and the emission spectrum of the pulse sampling function $S(t)$ is defined as

$$P_S(\omega) \equiv \frac{1}{\sqrt{2\pi}}\mathcal{F}(R_S(\tau)). \quad (31)$$

Equation (30) is the most important formula in this section, and we will use it to analyze the spectral features of the coherent radiation by fluctuating bunches. In the following discussion, we will discuss two mathematical models of the pulse sampling profile $S(t)$: impulsive sampling profile and rectangular sampling profile.

3.2.1 Impulsive sampling profile

If the pulse duration τ_b is much shorter than λ_b^{-1} , i.e., $\tau_b\lambda_b \ll 1$, the pulse profile $s(t)$ in Eq.(19) can be well described using the delta function $\delta(t)$, $s(t) \simeq \tau_b\delta(t)$ for $\tau_b \rightarrow 0$. According to Eq.(25) and Eq.(26), one has $r_s \simeq \tau_b^2\delta(\tau)$ and $q_s \simeq \tau_b$. Using Eq.(18) and Eq.(24), the autocorrelation function $R_S(\tau)$ of $S(t)$ is

$$R_S(\tau) = (\lambda_b\tau_b)^2 + \lambda_b\tau_b^2\delta(\tau). \quad (32)$$

According to Eq.(24) and Eq.(31), the emission spectrum of $S(t)$ is

$$P_S(\omega) = (\lambda_b\tau_b)^2\delta(\omega) + \frac{\lambda_b\tau_b^2}{2\pi}. \quad (33)$$

Therefore, based on Eq.(30), the emission spectrum of $\tilde{A}(t)$ is

$$P_{\tilde{A}}(\omega) = P_A(\omega) * P_S(\omega) = (\lambda_b\tau_b)^2P_A(\omega) + \frac{\lambda_b\tau_b^2}{2\pi}P_{A,\text{tot}}, \quad (34)$$

where $P_{A,\text{tot}}$ is the total radiation energy of $A(t)$,

$$P_{A,\text{tot}} = \int_{-\infty}^{\infty} P_A(\omega)d\omega. \quad (35)$$

Compared with that of a persistent bunch, $P_A(\omega)$, the emission spectrum of a fluctuating bunch is suppressed by a factor of $\sim (\lambda_b \tau_b)^2 = (\lambda_B \tau_B)^2$. For the scenario of an impulsive sampling profile, $\lambda_b \tau_b \ll 1$ has been potentially assumed. Meanwhile, the emission spectrum of a single fluctuating bunch is the sum of the emission spectrum of a persistent bunch and a white noise that is independent of frequency ω . The “signal-to-noise ratio” at the peak frequency ω_c in the frequency domain is given by

$$\left. \frac{S}{N} \right|_{\text{peak}} \simeq \frac{(\lambda_b \tau_b)^2 P_A(\omega_c)}{(\lambda_b \tau_b^2 / 2\pi) P_{A,\text{tot}}} = \frac{2\pi \lambda_b}{\omega_c}, \quad (36)$$

where $P_{A,\text{tot}} \sim \omega_c P_A(\omega_c)$ is adopted. The typical frequency bandwidth for classical curvature radiation is approximately $\omega_c \sim \gamma^3 c / \rho$. We can see that $(S/N)_{\text{peak}}$ is independent of τ_b , and the larger the pulse rate λ_b , the larger $(S/N)_{\text{peak}}$.

If one observes a non-white-noise signal in the frequency domain, i.e., $(S/N)_{\text{peak}} \gg 1$, $\lambda_b \gg \omega_c$ is required. For the GHz signal with $\omega_c / 2\pi \sim 10^9$ rad s⁻¹, the bunch formation rate should be $\lambda_b \gg 10^9$ s⁻¹, leading to $\lambda_B \simeq \lambda_b / 2\gamma^2 \gtrsim 10^3$ s⁻¹ γ_3^{-2} . In particular, for an FRB with a typical duration of a few milliseconds, at least one bunch is produced during $\Delta t \sim 1$ ms, leading to $\lambda_B \gtrsim 1/\Delta t \sim 10^3$ s⁻¹ and $\lambda_b \simeq 2\gamma^2 \lambda_B \gtrsim 10^9$ s⁻¹ $\gamma_3^2 \sim \omega_c$ and $(S/N)_{\text{peak}} \gtrsim 1$. Thus, the white-noise signal might not be significant for an FRB, if the FRB is produced by the bunch with a Lorentz factor $\gamma \gtrsim 10^3$. Notice that the above conclusion potentially assumes that $\tau_b \lambda_b \ll 1$ for the impulsive sampling profile.

3.2.2 Rectangular sampling profile

Next, we generally consider that the function $s(t)$ given by Eq.(19) could be well described by a rectangular profile with width τ_b , i.e.

$$s(t) = \text{rect}\left(\frac{t}{\tau_b}\right) \equiv \begin{cases} 1, & \text{for } \left|\frac{t}{\tau_b}\right| < \frac{1}{2}, \\ 0, & \text{for } \left|\frac{t}{\tau_b}\right| > \frac{1}{2}, \end{cases} \quad (37)$$

where $\text{rect}(x)$ is the rectangular function. The autocorrelation function $R_S(\tau)$ is

$$R_S(\tau) = (\lambda_b \tau_b)^2 + \lambda_b \tau_b \Lambda\left(\frac{\tau}{\tau_b}\right), \quad (38)$$

where $\Lambda(x)$ is the triangular function

$$\Lambda(x) \equiv \begin{cases} 1 - |x|, & \text{for } |x| \leq 1, \\ 0, & \text{otherwise.} \end{cases} \quad (39)$$

According to Eq.(24) and Eq.(31), the emission spectrum of $S(t)$ is

$$P_S(\omega) = (\lambda_b \tau_b)^2 \delta(\omega) + \frac{\lambda_b \tau_b^2}{2\pi} \text{sinc}^2\left(\frac{\tau_b \omega}{2}\right). \quad (40)$$

Using Eq.(30), the emission spectrum of $\tilde{A}(t)$ is

$$P_{\tilde{A}}(\omega) = (\lambda_b \tau_b)^2 P_A(\omega) + \frac{\lambda_b \tau_b^2}{2\pi} P_A(\omega) * \text{sinc}^2\left(\frac{\tau_b \omega}{2}\right). \quad (41)$$

Compared with that of a single persistent bunch, the emission spectrum of a fluctuating bunch is suppressed by a factor of $\sim (\lambda_b \tau_b)^2 = (\lambda_B \tau_B)^2$. The signal-to-noise ratio at the peak frequency in the frequency domain is given by

$$\left. \frac{S}{N} \right|_{\text{peak}} = \frac{2\pi \lambda_b P_A(\omega_c)}{P_A(\omega) * \text{sinc}^2(\tau_b \omega / 2)}. \quad (42)$$

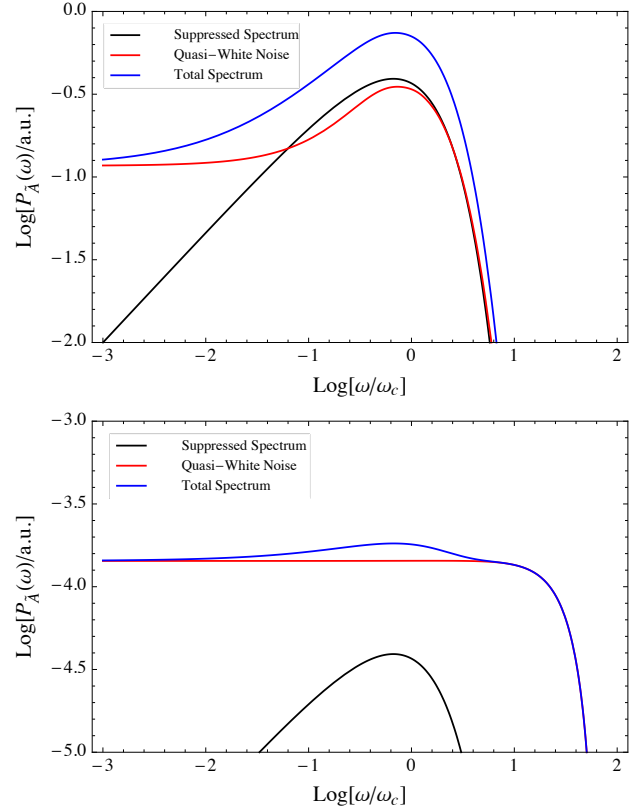


Figure 5. The emission spectrum of a single fluctuating bunch. The black, red, and blue curves correspond to the suppressed emission spectrum $(\lambda_b \tau_b)^2 P_A(\omega)$, the quasi-white noise $(\lambda_b \tau_b^2 / 2\pi) P_A(\omega) * \text{sinc}^2(\tau_b \omega / 2)$, and the total emission spectrum, respectively. The top panel is the case with $\lambda_b = 0.1 \omega_c$ and $\tau_b = 10 \omega_c^{-1}$, and the bottom panel is the case with $\lambda_b = 0.1 \omega_c$ and $\tau_b = 0.1 \omega_c^{-1}$. Here we take $P_A(\omega)$ as the emission spectrum of a single point source given by Eq.(10). The unit is arbitrary.

According to the property of the convolution of two pulse profiles, we have the following conclusions: (1) If $\tau_b > \omega_c^{-1}$, one has $(S/N)_{\text{peak}} \sim \lambda_b \tau_b = \lambda_B \tau_B$, and the cutoff frequency of the whole spectrum is at $\sim \omega_c$, see the top panel of Figure 5. (2) If $\tau_b < \omega_c^{-1}$, one has $(S/N)_{\text{peak}} \sim \lambda_b / \omega_c$, and there is a high-frequency cutoff in the white noise at $\tau_b^{-1} \sim \tilde{\omega}_c$, see the bottom panel of Figure 5. In particular, when $\tau_b \rightarrow 0$, one has $\text{sinc}^2(\tau_b \omega / 2) \sim 1$, so the above results become the case of an impulsive sampling profile as discussed in Section 3.2.1. In summary, for both cases, the cutoff frequency is at

$$\omega_{\text{cut}} \sim \max(\omega_c, \tau_b^{-1}), \quad (43)$$

and the signal-to-noise ratio at the peak frequency in the frequency domain is

$$\left. \frac{S}{N} \right|_{\text{peak}} \sim \frac{\lambda_b}{\min(\omega_c, \tau_b^{-1})}. \quad (44)$$

3.3 Radiation by multiple fluctuating bunches

Next, we discuss the radiation by multiple fluctuating bunches along a field line, that is, there is a bunch train (with more than one bunch) along the field line. We consider that the radiation by the first fluctuating bunch in the bunch train is $\tilde{A}(t)$, then the radiation by multiple

fluctuating bunches could be described as

$$\hat{A}(t) = \sum_j^N \tilde{A}(t - t_j), \quad (45)$$

where t_j is the arrival time of the pulse generated by the j -th bunch, and N is the total number of bunches along a field line. Since the generation process of a bunch has been considered to be a Poisson process, the radiation pulses from multiple fluctuating bunches also satisfy the Poisson distribution, i.e., $\{t_j\}$ satisfies $p_{t_j}(t) = \lambda_B P_{j-1}(t)$. Notice that here the rate of the Poisson process is the bunch formation rate, rather than the observed pulse rate λ_b , which is corrected for the propagation time-delay effect.

According to the time shifting property of Fourier transform, $\mathcal{F}[\tilde{A}(t - t_j)] = e^{i\omega t_j} \tilde{A}(\omega)$, the Fourier transform of $\hat{A}(t)$ is

$$\hat{A}(\omega) = \mathcal{F}[\hat{A}(t)] = \tilde{A}(\omega) \sum_j^N e^{i\omega t_j}. \quad (46)$$

Therefore, the emission spectrum of multiple fluctuating bunches is

$$\begin{aligned} P_{\hat{A}}(\omega) &= 2|\hat{A}(\omega)|^2 = 2|\tilde{A}(\omega)|^2 \left| \sum_j^N e^{i\omega t_j} \right|^2 \\ &= P_{\tilde{A}}(\omega) \left(N + \sum_{j \neq k} \sum e^{i\omega(t_j - t_k)} \right) = NP_{\tilde{A}}(\omega), \end{aligned} \quad (47)$$

where $\sum_{j \neq k} e^{i\omega(t_j - t_k)} \simeq 0$, because t_j and t_k are randomly distributed for the Poisson process. In conclusion, the radiation by multiple fluctuating bunches is the incoherent sum of that of each single fluctuating bunch, and the spectral shape of $P_{\hat{A}}(\omega)$ is the same as that of $P_{\tilde{A}}(\omega)$.

4 FORMATION AND DISPERSION OF FLUCTUATING BUNCHES

In this section, we will discuss the formation and dispersion mechanisms of bunches in a pulsar or magnetar magnetosphere and constrain λ_B and τ_B in various physical scenarios.

4.1 Bunch formation by two-stream instability

The most popular theory for the bunching mechanism in radio pulsars is that charged bunches are generated in the magnetosphere due to the two-stream instability developed by the interaction between two plasma components with different Lorentz factors (Ruderman & Sutherland 1975; Benford & Buschauer 1977; Cheng & Ruderman 1980; Usov 1987). A similar mechanism has also been proposed as a possible mechanism for FRBs (Kumar & Bošnjak 2020; Kumar et al. 2022). For an effective two-stream instability that is responsible for the observed radio emission, the typical timescale for the development of the two-stream instability, $\tau_\lambda = \lambda_B^{-1}$ in the pulsar frame should be shorter than the dynamical timescale of the plasma stream $\tau_0 = r/c$ at the distance r from a neutron star, i.e.

$$\tau_\lambda = \lambda_B^{-1} < \tau_0 = \frac{r}{c} = 3 \times 10^{-5} \text{ s } r_6. \quad (48)$$

We consider two plasma components with relative motion in the pulsar frame, which are denoted by “1” and “2”, respectively. Their typical Lorentz factors are γ_1 and γ_2 with $\gamma_1 > \gamma_2$, and their number densities are n_1 and n_2 with $n_1/\hat{\gamma}n_2 \ll 1$, where $\hat{\gamma} \simeq (1/2)(\gamma_1/\gamma_2 +$

$\gamma_2/\gamma_1) \simeq (1/2)(\gamma_1/\gamma_2)$ is the relative Lorentz factor. Then the one-dimensional electrostatic dispersion relation is given by (Benford & Buschauer 1977; Usov & Usov 1988),

$$1 - \frac{\omega_{p,2}^2}{\omega^2} - \frac{\omega_{p,1}^2}{\hat{\gamma}^3(\omega - k\hat{v})^2} = 0, \quad (49)$$

where $\omega_{p,j} = (4\pi en_j/m_e)^{1/2}$ is the plasma frequency of the component j , \hat{v} is the relative velocity between the two plasma components with $\hat{\gamma} = (1 - \hat{v}^2/c^2)^{-1/2}$, and k is the wavevector of the electrostatic wave. According to this dispersion relation, the typical timescale for the development of a two-stream instability in the pulsar frame is (Benford & Buschauer 1977; Usov 1987)

$$\tau_\lambda \sim [\text{Im}(\omega_{\text{max}})]^{-1} \sim \left(\frac{n_2}{n_1}\right)^{1/3} \gamma_1 \gamma_2^{1/2} \omega_{p,2}^{-1}, \quad (50)$$

where $\text{Im}(\omega_{\text{max}})$ corresponds to the fastest growth rate obtained by dispersion relation.

First, we discuss the two-stream instability caused by the relative motion between an ultrarelativistic beam plasma and a relativistic cascade pair plasma. Generally, the plasma that flows out from the pulsar can be divided into two components: (1) An ultrarelativistic primary beam (denoted by u) that is directly accelerated by the charge-starved regions named “gaps”. It has a typical Lorentz factor γ_u and a density n_u ; (2) A relativistic electron-positron plasma (denoted by \pm) that is produced by the pair cascade process. It has a typical Lorentz factor $\gamma_\pm \ll \gamma_u$ and a density is

$$n_\pm \simeq \left(\frac{\gamma_u}{2\gamma_\pm}\right) n_u. \quad (51)$$

The number density of the primary ultrarelativistic beam should generally follow the number density of net charges in the magnetosphere. There are two scenarios for the magnetosphere of a neutron star: (1) If the magnetosphere is non-twisting, the number density of net charges is the Goldreich-Julian density (Goldreich & Julian 1969),

$$n_{\text{GJ}} \equiv \frac{\Omega B(r)}{2\pi e c}, \quad (52)$$

where $B(r) = B_p(r/R_n)^{-3}$ is the strength of a dipole field at the distance r , B_p is the surface magnetic field, R_n is the neutron star radius, and Ω is the neutron star angular velocity. (2) If the magnetosphere is twisted during an activity (e.g. a magnetar activity), the number density of net charges is

$$n_{\text{twist}} \equiv \frac{1}{4\pi e} \nabla \times \mathbf{B} \sim \frac{B(r)}{4\pi e r} \sin^2 \theta \Delta\phi, \quad (53)$$

where θ is the poloidal angle and $\Delta\phi$ is the twisting angle of the field. Generally, for a certain neutron star, one usually has

$$n_u \sim \max(n_{\text{GJ}}, n_{\text{twist}}). \quad (54)$$

According to Eq.(50), the typical timescale for the development of the two-stream instability in the pulsar frame is

$$\tau_\lambda \sim \left(\frac{n_\pm}{n_u}\right)^{1/3} \gamma_u \gamma_\pm^{1/2} \omega_p^{-1}, \quad (55)$$

where $\omega_p = (4\pi e^2 n_\pm/m_e)^{1/2}$ is the pair plasma frequency. For the typical parameters of a pulsar with a non-twisting magnetosphere, the two-stream instability for such a stationary environment may not have enough time to develop, i.e., $\tau_\lambda > \tau_0$ (Usov 1987). Here, we are mainly interested in the scenario of the twisted magnetosphere of a magnetar, in which case, the number density of charged particles in

the magnetosphere is large enough, leading to a larger growth rate for the two-stream instability.

We consider that a magnetar has the surface magnetic field $B_p \sim 10^{14}$ G, rotation period $P \sim 0.1$ s and twisting angle $\Delta\phi \sim 0.1$. We take a polar angle $\sin^2\theta \sim 0.1$, and the two components of the outflowing plasmas have Lorentz factors of $\gamma_u \sim 10^5$ and $\gamma_{\pm} \sim 100$, respectively. Because $n_{\text{twisting}} \gg n_{\text{GJ}}$, one has $n_u = n_{\text{twisting}} \sim 1.6 \times 10^{14} \text{ cm}^{-3} r_6^{-4}$ and $n_{\pm} = (\gamma_u/2\gamma_{\pm})n_u \sim 8.3 \times 10^{16} \text{ cm}^{-3} r_6^{-4}$. Thus, the timescale for the development of a two-stream instability is $\tau_{\lambda} \sim 4.9 \times 10^{-7} \text{ s } r_6^2$. According to the condition of $\tau_{\lambda} < \tau_0$, the instability would develop within the distance of $r \sim (10^7 - 10^8)$ cm. Since $\omega > \omega_p/\sqrt{\gamma_{\pm}}$ at $r \sim (10^7 - 10^8)$ cm, the plasma environment would be transparent for GHz wave².

The transparency condition $\omega > \omega_p/\sqrt{\gamma_{\min}}$ can give a general constraint on the instability timescale,

$$\tau_{\lambda} > \gamma_u^{4/3} \gamma_{\pm}^{-1/3} \omega^{-1}. \quad (56)$$

For example, we consider that $\gamma_u \sim 10^5$, $\gamma_{\pm} \sim 100$, and $\omega/2\pi \sim 10^9 \text{ rad s}^{-1}$, then the timescale of the two-stream instability is constrained to be $\tau_{\lambda} > 1.6 \times 10^{-4}$ s. Using the condition of $\tau_{\lambda} < \tau_0 = r/c$, the bunching formation region should be at $r > (10^6 - 10^7)$ cm. One also has $\lambda_B < 6.3 \times 10^3 \text{ s}^{-1}$ and $\lambda_b \lesssim 2\gamma_{\pm}^2 \lambda_B \approx 1.2 \times 10^8 \text{ s}^{-1}$. Since $(S/N)_{\text{peak}} = 2\pi\lambda_b/\omega_c \ll 1$ for GHz wave with $\omega_c/2\pi \sim 10^9 \text{ rad s}^{-1}$, the corresponding spectrum would appear as white-noise in the frequency domain.

Another possibility for the development of a two-stream instability is due to the non-stationarity of the plasma stream (Usov 1987; Usov & Usov 1988). In this case, the pair plasma that flows out from the pulsar is inhomogeneous and can gather into separate clouds along the field lines. We consider that the Lorentz factors of the electron/positrons in the pair plasma have a wide range distribution from γ_{\min} up to γ_{\max} , so the pair clouds disperse as they flow out from the pulsar. The energy distribution of the plasma particles satisfies

$$n(\gamma)d\gamma = n_{\gamma}\gamma^{-p}d\gamma \quad (57)$$

with $n_{\gamma} \equiv (p-1)\gamma_{\min}^{p-1}n_{\pm}$, where n_{\pm} is the total pair number density. At the interaction distance r_i , the high-energy particles with $\gamma \sim \gamma_{\max}$ of a cloud B catch up with the low-energy particles with $\gamma \sim \gamma_{\min}$ of the cloud A in front of the cloud B with an initial separation L . The interaction distance is

$$r_i = \frac{L}{v_{\max} - v_{\min}} \approx 2\gamma_{\min}^2 L \quad (58)$$

for $\gamma_{\max} \gg \gamma_{\min} \gg 1$, where v_{\min} and v_{\max} are the particle minimum and maximum velocities, respectively. Here we briefly assume that cloud A and B have the same number densities.

At the distance r_i , there are only particles with $\gamma \sim \gamma_{\min}$ and $\gamma \sim \gamma_{\max}$ in the merged cloud, so the two-stream instability could develop. Component 1 has density $\sim \gamma_{\max}n(\gamma_{\max})$ and Lorentz factor γ_{\max} , and Component 2 has density $\sim \gamma_{\min}n(\gamma_{\min})$ and Lorentz factor γ_{\min} . Therefore, the typical timescale for the development of the two-stream instability in the pulsar frame is

$$\tau_{\lambda} \sim \gamma_{\min}^{\frac{5-2p}{6}} \gamma_{\max}^{\frac{2+p}{3}} \omega_p^{-1} \quad (59)$$

with $\omega_p = \sqrt{4\pi n_e/m_e}$ and $n_e \sim \gamma_{\min}n(\gamma_{\min})$. For a magnetar with the above parameters, the pair number density is $n_{\pm} \sim$

$8.3 \times 10^{16} \text{ cm}^{-3} r_6^{-4}$ and $n_e \sim \gamma_{\min}n(\gamma_{\min}) \sim n_{\pm}$. We consider that $\gamma_{\min} \sim 100$, $\gamma_{\max} \sim 10^4$ and $p \sim 2.5$. Thus, the timescale for the development of the two-stream instability is $\tau_{\lambda} \sim 6.2 \times 10^{-8} \text{ s } r_6^2$. The instability would develop within $r \sim (10^8 - 10^9)$ cm. Because $\omega > \omega_p/\sqrt{\gamma_{\min}}$ at $r \sim (10^8 - 10^9)$ cm, the plasma environment would be transparent to GHz wave.

For an electromagnetic wave with angular frequency ω , the transparency condition requires $\omega > \omega_p/\sqrt{\gamma_{\min}}$, leading to

$$\tau_{\lambda} > \gamma_{\min}^{\frac{1-p}{3}} \gamma_{\max}^{\frac{2+p}{3}} \omega^{-1}. \quad (60)$$

For the above typical parameters, the timescale of the two-stream instability is constrained to be $\tau_{\lambda} > 1.6 \times 10^{-5}$ s, leading to $\lambda_B < 6.3 \times 10^4 \text{ s}^{-1}$ and $\lambda_b \lesssim 2\gamma_{\min}^2 \lambda_B = 1.2 \times 10^9 \text{ s}^{-1}$. Since $(S/N)_{\text{peak}} = 2\pi\lambda_b/\omega_c \sim 1$ is allowed for GHz waves with $\omega_c/2\pi \sim 10^9 \text{ rad s}^{-1}$, the corresponding spectrum would be non-white-noise in the frequency domain. On the other hand, since $\tau_{\lambda} < \tau_0$ is allowed at $r > 10^6$ cm, the two-stream instability can develop.

In addition to the above scenarios, very recently Kumar et al. (2022) found that a two-stream-like instability can develop via the interaction between a charge-carrying Alfvén wave and a stationary medium, and the corresponding growth rate is of order the plasma frequency of the medium encountered by the charge-carrying Alfvén wave. This mechanism can cause the emergence of a strong electric field along the direction of the magnetic field that is of the order of a few percent of the Alfvén amplitude.

4.2 Bunch dispersion mechanism

Since the bunches in the magnetosphere are charged, over-dense, and composed of particles with different velocities, they will be dispersed some times after they form. For a plasma fluid, the decay rate is usually of the order of the growth rate, thus the typical lifetime of a bunch is $\tau_B \sim \lambda_B^{-1}$. According to Section 3.2, the emission spectrum of a fluctuating bunch is suppressed by a factor of $\sim (\lambda_b\tau_b)^2 = (\lambda_B\tau_B)^2$ compared with that of a persistent bunch. Thus $\tau_B \sim \lambda_B^{-1}$ implies that the emission spectrum of a fluctuating bunch is not significantly suppressed by plasma fluctuations. However, some extreme mechanisms, e.g. velocity dispersion, electrostatic repulsion, radiation cooling, etc., may cause $\tau_B \ll \lambda_B^{-1}$, leading to the suppression of the emission spectrum.

For example, due to the two-stream instability that involves two fluid components with different velocities, the relativistic particles in a bunch usually have a Lorentz factor dispersion $\Delta\gamma$. We consider the average velocity of the particles being v with Lorentz factor $\gamma = (1 - v^2/c^2)^{-1/2}$. Then the velocity dispersion of the relativistic particles is $\Delta v \sim c\Delta\gamma/\gamma^3$, which causes a linear extent of the bunch during time t

$$\Delta l \sim \Delta vt \sim \frac{ct}{\gamma^2} \quad (61)$$

for $\Delta\gamma \sim \gamma$. For an electromagnetic wave with typical frequency ν_0 , a significant coherence requires $\Delta l \lesssim c/\nu_0$. Otherwise, the radiation would be suppressed (Yang & Zhang 2018b). Thus, the bunch lifetime is constrained by

$$\tau_B \sim t \lesssim \frac{\gamma^2}{\nu_0}, \quad (62)$$

leading to $\tau_b \approx \tau_B/(2\gamma^2) \lesssim \nu_0^{-1} \sim \omega_c^{-1}$ for $\nu_0 \sim \omega_c$.

The bunch dispersion can be also caused by electrostatic repulsion. We consider that the bunch has a charge density ρ , total charge Q ,

² Notice that in the work, the transparency condition of the electromagnetic waves does not involve the non-linear plasma effect of strong waves, which would cause a much lower plasma oscillation frequency but a larger scattering opacity (Yang & Zhang 2020; Beloborodov 2022; Qu et al. 2022).

length l , width b , and Lorentz factor γ . Due to the magnetosphere rotation, the stationary charge density distribution is the Goldreich-Julian density (Goldreich & Julian 1969), and only the fluctuating density with $\delta\rho = \rho - \rho_{\text{GJ}} > 0$ would be affected by the electrostatic repulsion, where $\rho_{\text{GJ}} = \Omega B/2\pi c$. The bunch expands along the field line due to the binding of the magnetic field. In the bunch comoving frame corrected by the magnetosphere rotation, a charged particle in the bunch end is acted by the electrostatic force

$$m_e \frac{l'}{\tau_{\text{rep}}^2} \sim \frac{\delta Q e}{l'^2} \sim \frac{\delta Q e}{l' b^2} \frac{b^2}{l'} \sim e \delta \rho' \frac{b^2}{l'}, \quad (63)$$

where $\delta Q = Q - Q_{\text{GJ}}$ is the bunch total charge deducting the Goldreich-Julian charge contribution, the quantities labeled by a prime are in the bunch comoving frame, τ_{rep} is the typical repulsion timescale in the bunch comoving frame, l'/τ_{rep} is the typical acceleration of the particle in Newton's second law. Therefore, the typical repulsion timescale in the pulsar frame is

$$\tau_{\text{rep}} \sim \gamma \tau'_{\text{rep}} \sim \gamma^2 \left(\frac{\gamma m_e}{e \delta \rho} \right)^{1/2} \frac{l}{b}, \quad (64)$$

where the relativistic transformations of $\delta \rho' \sim \delta \rho / \gamma$ and $l' \sim \gamma l$ are used. If we further assume that the bunch is approximately isotropic in the comoving frame, $l' \sim b$, one would have $l/b \sim 1/\gamma$, leading to

$$\tau_{\text{rep}} \sim \gamma \left(\frac{\gamma m_e}{e \delta \rho} \right)^{1/2} \approx 6.3 \times 10^{-8} \text{ s } \gamma_2^{3/2} \delta n_{12}^{-1/2}, \quad (65)$$

where $\delta n = \delta \rho / e$. According to the transparency condition $\omega > \omega_p / \sqrt{\gamma}$ with $\omega_p = (4\pi e \kappa \rho / m_e)^{1/2}$ and $\delta \rho \sim \rho$, where κ is the pair multiplicity, the repulsion timescale could be constrained by

$$\tau_{\text{rep}} > \frac{(4\pi \kappa)^{1/2} \gamma}{\omega}. \quad (66)$$

For $\omega/2\pi \sim 10^9 \text{ rad s}^{-1}$, $\gamma \sim 100$ and $\kappa \sim 10^4$, one has $\tau_{\text{rep}} > 5.6 \times 10^{-6} \text{ s}$.

Another possibility is that the bunches are fast cooling by the radiation reaction. Due to the large coherent radiation power, the bunches likely cool rapidly within a very short timescale. For simplicity, we consider a bunch as a point source with a net charge number N , the radiation power of coherent curvature radiation is

$$P_c = N^2 \frac{2e^2 c \gamma^4}{3\rho^2}. \quad (67)$$

Thus, the isotropic equivalent luminosity is given by

$$L_{\text{iso}} \sim \gamma^4 N_{\text{patch}} P_c \sim N_{\text{patch}} N^2 \frac{2e^2 c \gamma^8}{3\rho^2}, \quad (68)$$

where N_{patch} is the number of coherent patches, the factor of γ^4 is attributed to the radiation beaming effect and the retarded time corrected by the relativistic propagation effect (Kumar et al. 2017). If the radiation energy is mainly from the kinetic energy of the charged particles in the bunch, the cooling time is

$$\begin{aligned} \tau_{\text{cool}} &\sim \frac{N \gamma m_e c^2}{P_c} \sim \frac{3m_e c^2 \rho}{2e^2 \omega_c N} \sim \frac{3^{1/2} m_e c^5/2 \gamma^4 N_{\text{patch}}^{1/2}}{2^{1/2} e \omega_c L_{\text{iso}}^{1/2}} \\ &\approx 5.8 \times 10^{-14} \text{ s } \gamma_2^4 N_{\text{patch}}^{1/2} \gamma_{c,9}^{-1} L_{\text{iso},40}^{-1/2}, \end{aligned} \quad (69)$$

where $\omega_c \sim \gamma^3 c / \rho$ is used. Thus, the cooling time of a charged bunch could be very short for ranging from radio pulsars with $L_{\text{iso}} \sim 10^{30} \text{ erg s}^{-1}$ and FRBs with $L_{\text{iso}} \sim 10^{40} \text{ erg s}^{-1}$. However,

this discussion assumes that the radiation is mainly from the particle kinetic energy $N \gamma m_e c^2$. For pulsars and especially for FRBs, the radio emission is usually believed to be generated at the charge-starved region where there exists an electric field parallel to the local magnetic field with an energy density $U_E \sim E^2/8\pi \gg \gamma m_e c^2 n_e$, where n_e is the electron number density. (Ruderman & Sutherland 1975; Kumar et al. 2017, 2022). The parallel electric field accelerates the charged bunches and cancels the dispersion due to radiative cooling, leading to a much longer longer cooling time.

5 CONCLUSIONS AND DISCUSSIONS

Although coherent curvature radiation by charged bunches has been proposed to explain the coherent emissions of radio pulsars and FRBs, this mechanism still encounters some issues, including how the charged bunches form and disperse and what the radiation features are for the case of fluctuating bunches in the emission region. In this work, we consider that the bunches in a neutron star magnetosphere form with an average rate of λ_B and have an average lifetime of τ_B . We mainly analyze the spectral features of coherent curvature radiation by dynamically fluctuating bunches and discuss some possible physical mechanisms for the formation and dispersion of the charged bunches in the magnetosphere of a neutron star. The following conclusions are drawn:

1. We first point out that the classical formula of calculating the brightness temperature of FRB emission, i.e. Eq.(2), that involves the transient duration Δt is not applicable to the scenario of the magnetospheric curvature radiation, because Δt does not directly reflect the transverse size l_e of the emission region for curvature radiation. Considering that the charged bunches move along the field line with a Lorentz factor γ at a distance r from the neutron star center, the transverse size of the emission region is estimated as $l_e \sim r/\gamma$ for $\omega \sim \omega_c$, leading to $l_e \ll c\Delta t$. Therefore, for the typical parameters of the magnetosphere, the brightness temperature should be much larger than that given by Eq.(2).

2. The classical theory of curvature radiation potentially assumes that the bunch lifetime satisfies $\tau_B > \rho/\gamma c$, where ρ is the curvature radius and γ is the bunch Lorentz factor. Both the typical frequency and the cutoff frequency are $\omega_c \sim \gamma^3 c/\rho$ and the spectral feature depends on the spatial structure of the bunch. For example, we consider that the bunch has a lengthscale of l . Compared with the radiation spectrum of a single point-charge persistent bunch, the radiation spectrum by an extending bunch is corrected by a factor of $\text{sinc}^2(\omega/\omega_l)$ with $\omega_l \sim 2c/l$, and the radiation power is suppressed by a factor of $(\omega_l/\omega_c)^{5/3}$. In particular, since the excess of one charge is usually compensated by the lack of this charge in the nearby regions, a bunch-cavity system might form in the magnetosphere. It has an emission spectrum much narrower than that of a single persistent bunch and with the emission spectrum of $P_A(\omega) \propto \omega^{8/3}$ in the low-frequency band.

3. If the bunch lifetime is short enough, $\tau_B < \rho/\gamma c$, the cutoff frequency would become $\tilde{\omega} \sim \gamma^2/\tau_B \gtrsim \omega_c$. Thus, a short-lived bunch will radiate electromagnetic waves with a higher frequency compared with that of classical curvature radiation. Considering that bunches form and disperse intermittently when the building plasma particles move along a magnetic field line, the emission spectrum of such a fluctuating bunch is a convolution between the emission spectrum of a single persistent bunch $P_A(\omega)$ and that of the pulse sampling function $P_S(\omega)$, $P_{\tilde{A}}(\omega) = P_A(\omega) * P_S(\omega)$, where $P_S(\omega)$ is the emission spectrum of the pulse sampling function $S(t)$ that is described by Eq. (18) and Figure 4.

4. According to the above point, we obtained the emission spectrum of a single fluctuating bunch, $P_{\bar{A}}(\omega)$. We find that compared with that of a single fluctuating bunch, $P_{\bar{A}}(\omega)$ is suppressed by a factor of $(\lambda_b \tau_b)^2$, where $\lambda_b \approx 2\gamma^2 \lambda_B$ and $\tau_b \approx \tau_B/2\gamma^2$ are the pulse rate and duration, respectively, λ_B and τ_B are the bunch formation rate and lifetime, respectively, and the factor of $2\gamma^2$ is corrected by the propagation time-delay effect. Meanwhile, there is a quasi-white noise in the wider band. We define $(S/N)_{\text{peak}}$ as the ‘‘signal-to-noise ratio’’ at the peak frequency ω_c in the frequency domain, and $(S/N)_{\text{peak}} \gtrsim 1$ means that the spectrum is non-white-noise. If $\tau_b < \omega_c^{-1}$, where $\omega_c \sim \gamma^3 c/\rho$ is the typical frequency of the classical curvature radiation, one has $(S/N)_{\text{peak}} \sim \lambda_b/\omega_c$, and there is a high-frequency cutoff in the white noise at $\tilde{\omega}_c \sim \tau_b^{-1}$. If $\tau_b > \omega_c^{-1}$, one has $(S/N)_{\text{peak}} \sim \lambda_b \tau_b = \lambda_B \tau_B$, the cutoff frequency of the whole spectrum is at $\sim \omega_c$.

5. If there are multiple fluctuating bunches along a field line, the emission spectrum of multiple fluctuating bunches is the incoherent sum of that of each single fluctuating bunch because the separation between adjacent bunch is randomly distributed. In this scenario, the spectral shape is the same as that of single fluctuating bunches, and the total radiation power is incoherently enhanced.

6. We briefly discussed some mechanisms for bunch formation and dispersion. Since the radiation power of a fluctuating bunch is suppressed by a factor $(\lambda_B \tau_B)^2$, if the coherent radiation power by bunch fluctuation is not significant, the condition $(\lambda_B \tau_B)^2 \sim 1$ should be satisfied. Generally, for a plasma instability, the decay rate is usually of the order of the growth rate, leading to $(\lambda_B \tau_B)^2 \sim 1$. However, some extreme mechanisms, e.g. velocity dispersion, electrostatic repulsion, and radiation cooling may cause $\tau_B \ll \lambda_B^{-1}$, which might cause the radiation power to be suppressed. On the other hand, if the observed spectrum is non-white-noise, the condition of $(S/N)_{\text{peak}} \gtrsim 1$ causes $\lambda_b \gtrsim \min(\omega_c, \tau_b^{-1})$, leading to $\lambda_B \sim \omega_c/2\gamma^2 \approx 3 \times 10^5 \text{ s}^{-1} \nu_{c,9} \gamma_2^{-2}$ for $\omega_c < \tau_b^{-1}$.

At last, we also notice that the theory of the spectral analysis for fluctuating bunches not only applies to curvature radiation but also to coherent inverse Compton scattering (ICS) by charged bunches (Zhang 2022b). This mechanism generally has a much higher radiation power than curvature radiation, so that a lower degree of coherence is needed to interpret FRBs. Similar to the scenario of curvature radiation, a white-noise component in the emission spectrum would also appear due to bunch fluctuations. Compared with coherent curvature radiation, the major difference is that the emission spectrum of coherent ICS mainly depends on the properties of the incident electromagnetic waves which should be involved in the discussion of the emission of a single persistent bunch. On the other hand, since the radiation direction of coherent ICS is also along the magnetic field line due to the relativistic motion of the bunches, its emission spectrum might be modulated by the typical frequency ω_c . A detailed analysis of this mechanism will be performed in the future.

ACKNOWLEDGEMENTS

We thank Qiao-Chu Li for the constructive discussion about the signal theory. Y-PY’s work is supported by the National Natural Science Foundation of China grant No.12003028, the National Key Research and Development Program of China (2022SKA0130101), and the China Manned Space Project (CMS-CSST-2021-B11).

DATA AVAILABILITY

This theoretical study did not generate any new data.

REFERENCES

- Bailes M., 2022, *Science*, **378**, abj3043
 Basu R., Mitra D., Melikidze G. I., 2022, *ApJ*, **927**, 208
 Beloborodov A. M., 2022, *Phys. Rev. Lett.*, **128**, 255003
 Benford G., Buschauer R., 1977, *MNRAS*, **179**, 189
 Buschauer R., Benford G., 1976, *MNRAS*, **177**, 109
 Cheng A. F., Ruderman M. A., 1980, *ApJ*, **235**, 576
 Cooper A. J., Wijers R. A. M. J., 2021, *MNRAS*, **508**, L32
 Cordes J. M., Chatterjee S., 2019, *ARA&A*, **57**, 417
 Franks L. E., 1981, *Signal Theory (Revised Edition)*
 Gil J., Lyubarsky Y., Melikidze G. I., 2004, *ApJ*, **600**, 872
 Ginzburg V. L., Zhelezniakov V. V., 1975, *ARA&A*, **13**, 511
 Goldreich P., Julian W. H., 1969, *ApJ*, **157**, 869
 Jackson J. D., 1998, *Classical Electrodynamics*, 3rd Edition
 Katz J. I., 2014, *Phys. Rev. D*, **89**, 103009
 Katz J. I., 2018, *MNRAS*, **481**, 2946
 Kumar P., Bošnjak Ž., 2020, *MNRAS*, **494**, 2385
 Kumar P., Lu W., Bhattacharya M., 2017, *MNRAS*, **468**, 2726
 Kumar P., Gill R., Lu W., 2022, *MNRAS*, **516**, 2697
 Liu Z.-N., Wang W.-Y., Yang Y.-P., Dai Z.-G., 2022, *arXiv e-prints*, p. arXiv:2212.13153
 Lu W., Kumar P., 2018, *MNRAS*, **477**, 2470
 Lu W., Kumar P., Zhang B., 2020, *MNRAS*, **498**, 1397
 Luo J.-W., Zhu-Ge J.-M., Zhang B., 2023, *MNRAS*, **518**, 1629
 Lyubarsky Y., 2021, *Universe*, **7**, 56
 Melikidze G. I., Gil J. A., Pataraya A. D., 2000, *ApJ*, **544**, 1081
 Melrose D. B., 2017, *Reviews of Modern Plasma Physics*, **1**, 5
 Petroff E., Hessels J. W. T., Lorimer D. R., 2019, *A&ARv*, **27**, 4
 Qu Y., Kumar P., Zhang B., 2022, *MNRAS*, **515**, 2020
 Qu Y., Zhang B., Kumar P., 2023, *MNRAS*, **518**, 66
 Ruderman M., 1971, *Phys. Rev. Lett.*, **27**, 1306
 Ruderman M. A., Sutherland P. G., 1975, *ApJ*, **196**, 51
 Sturrock P. A., 1971, *ApJ*, **164**, 529
 Tong H., Wang H.-G., 2022, *Research in Astronomy and Astrophysics*, **22**, 075013
 Ursov V. N., Usov V. V., 1988, *Ap&SS*, **140**, 325
 Usov V. V., 1987, *ApJ*, **320**, 333
 Wang W.-Y., Jiang J.-C., Lee K., Xu R., Zhang B., 2022a, *MNRAS*, **517**, 5080
 Wang W.-Y., Yang Y.-P., Niu C.-H., Xu R., Zhang B., 2022b, *ApJ*, **927**, 105
 Xiao D., Dai Z.-G., 2022, *A&A*, **657**, L7
 Xiao D., Wang F., Dai Z., 2021, *Science China Physics, Mechanics, and Astronomy*, **64**, 249501
 Yang Y.-P., Zhang B., 2018a, *ApJ*, **864**, L16
 Yang Y.-P., Zhang B., 2018b, *ApJ*, **868**, 31
 Yang Y.-P., Zhang B., 2020, *ApJ*, **892**, L10
 Yang Y.-P., Zhu J.-P., Zhang B., Wu X.-F., 2020, *ApJ*, **901**, L13
 Zhang B., 2020, *Nature*, **587**, 45
 Zhang B., 2022a, *arXiv e-prints*, p. arXiv:2212.03972
 Zhang B., 2022b, *ApJ*, **925**, 53
 Zhu-Ge J.-M., Luo J.-W., Zhang B., 2023, *MNRAS*, **519**, 1823

This paper has been typeset from a $\text{\TeX}/\text{\LaTeX}$ file prepared by the author.